Available online at www.sciencedirect.com
ScienceDirect
International Journal of Multiphase Flow 32 (2006) 889–901
International Journal of Multiphase Flow
www.elsevier.com/locate/ijmulflow

Flow patterns and heat transfer in vertical upward air–water flow with surfactant

R. Rozenblit, M. Gurevich, Y. Lengel, G. Hetsroni *

Department of Mechanical Engineering, Technion-IIT, 32000 Haifa, Israel

Received 23 November 2005; received in revised form 9 March 2006

Abstract

Flow patterns, the pressure drag reduction and the heat transfer in a vertical upward air–water flow with the surfactant having negligible environmental impact were studied experimentally in a tube of 2.5 cm in diameter. Visual observations showed that gas bubbles in the air–water solution with surfactant are smaller in size but much larger in number than in pure air–water mixture, at the all flow regimes. The transition lines in the flow regime map for the solution of air–water mixture with surfactant of the 300 ppm concentration are mainly consistent with the experimental data obtained in clear air–water mixture. An additive of surfactant to two-phase flow reduces the total pressure drop and decrease heat transfer, especially in the churn flow regime.

Keywords: Air–water flow; Surfactant; Flow regime; Pressure drag reduction; Heat transfer

1. Introduction

It is well known that an addition of very small amount of drag reducing agents (DRA) to single phase turbulent flow causes a drastic decrease in the friction factor (Virk, 1975), which results in the reduction of the pressure drop in tubes and channels. Several works (Soleimani et al., 2002; Baik and Hanratty, 2003; Al-Sarkhi and Soleimani, 2004) have shown that in two-phase horizontal flows the additive of DRA may change not only the pressure drop but the flow pattern as well. The latter study reported the effect of a drag-reducing polymer on two-phase flow patterns in a horizontal of 0.0254 m pipe. It was noted that the interfacial shear stress was decreased sharply and the flow pattern map was changed. The pressure drop reduction occurred in almost all flow pattern configurations. This study indicates that maximum drag reduction usually took place when a slug, pseudo-slug or annular flow changed to a stratified flow by adding DRA.

There are very few studies on effect of DRA in two-phase vertical flows, in spite of the importance of this problem in long heated pipe systems. The effect of such DRA as Separan AP on downward co-current annular

* Corresponding author. Tel.: +972 48 292 058; fax: +972 48 238 101.
E-mail address: hetsroni@tx.technion.ac.il (G. Hetsroni).

0301-9322/$ - see front matter © 2006 Elsevier Ltd. All rights reserved.
doi:10.1016/j.ijmultiphaseflow.2006.03.003

flow in a 31.8 mm diameter pipe was studied by Thwaites et al. (1976). They reported that the surfactant caused a significant reduction in pressure drop and wave frequency. Sawai et al. (2004) studied the effect of surfactant additives on pressure drop and flow pattern in a vertical upward two-phase flow. The experimental studies were conducted for two types of surfactants: one was *n*-hexadecyltrimethylammonium chloride mixed with a counter-ion sodium salicylate (CTAC) and the other was sodium oleate (SO). The surface tension was reduced up to 50% of that of water by addition of each surfactant. The pressure drop reduction (PDR) was achieved up to 90% by the addition of CTAC at liquid volumetric flux of 0.002 m/s. When SO was added, the PDR obtained was up to 40% in the annular flow at low liquid volumetric flux. Both surfactants caused little effect on the flow pattern transition between slug and churn/annular flows, but the churn flow regime was significantly affected by the addition of CTAC. The flow pattern transition between bubble and slug flows was only slightly affected by the surfactant addition.

Several maps of two-phase flow patterns have been proposed (see e.g. Taitel et al., 1980; Ohnuki and Akimoto, 1996; Spedding et al., 1998). The heat transfer and pressure fluctuations depend on the flow pattern. Hetsroni and Rozenblit (2000) related the near-wall flow structure in air–water flow to the heat transfer coefficient by using a heated foil infrared technique. They reported that for bubble flow the near wall streaky structure (this structure is typical to turbulent single-phase flow) is destroyed. This phenomenon is accompanied by a significant increase in the heat transfer whereas the level of pressure fluctuations at the wall almost did not change. For slug flow, the temperature distribution on the heated wall depends strongly on whether slug or water surrounding the Taylor bubble, passes on the heated wall at any instant. The level of pressure fluctuation increases when the relation of superficial velocities of gas and liquid increases.

An additive of surfactants changes the surface tension of the carrying fluid and the pressure drop per unit length in pipes and channels. Unfortunately, most of surfactants are not suited for industrial systems because of their degradation and environmental impact. That is why we have begun a study on hydrodynamics and heat transfer in heated tubes by adding alkyl polyglycosides to the flow in spite of the fact that their drag-reducing performance is not the best compared to others surfactants. Alkyl polyglycosides are nonionic surfactants with negligible environmental impact (Von Rybinski and Hill, 1998). Their production from the renewable resources glucose and fatty alcohol and their ultimate biodegradation is an example for a closed cycle. We used an Alkyl (8–16) Glucoside with molecular weight of 390 g/mol for our experiments.

This work is aimed at revealing the effect of surfactant on the flow pattern transition, drag reduction and heat transfer in a vertical air–water flow.

2. Experimental

2.1. Rheological properties of surfactant solutions

The solution was prepared by dissolving the surfactant (52% active substance and 48% water) in deionized water, with a gentle stirring over a period of a one-day. The main physical properties can be found in Hetsroni et al. (2004). The shear viscosity of the surfactant solution for two temperatures at various concentrations is shown in Fig. 1. The measurements of surface tension were carried out for different concentrations of surfactant solutions over a range of temperature from 300 to 368 K with standard deviation of 2%. In Fig. 2 the equilibrium surface tension, σ, is plotted versus the concentration of the surfactant solution at different temperatures. An increase in the surfactant concentration up to $C = 300$ ppm (parts per million weight) leads to significant decrease in the surface tension, whereas the surface tension is almost independent of concentration in the range $300 \leqslant C \leqslant 1200$ ppm. In all cases an increase in a liquid temperature leads to a decrease in the surface tension.

2.2. Experimental set-up

Experiments were carried out for a vertical upward air–water flow in a circular pipe of inner diameter 24.2 mm. A schematic diagram of the loop is shown in Fig. 3. The overall height of the setup is 12 m. It includes an 8 m long entrance section (about 330 tube diameters), which makes it possible to obtain a fully developed flow in the test section. The water was supplied to the test section from the entrance tank, 1, by

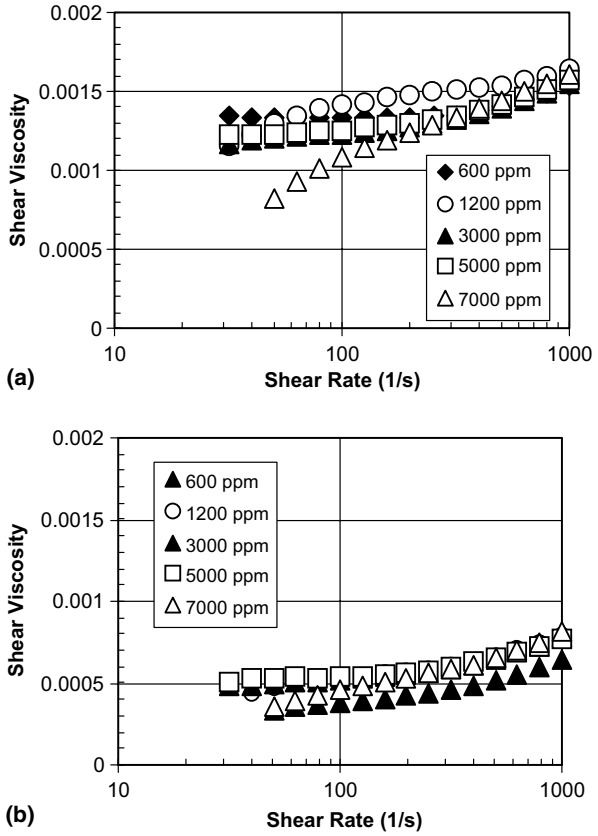

Fig. 1. The shear viscosity of the surfactant solution: (a) $T = 25$ °C and (b) $T = 60$ °C.

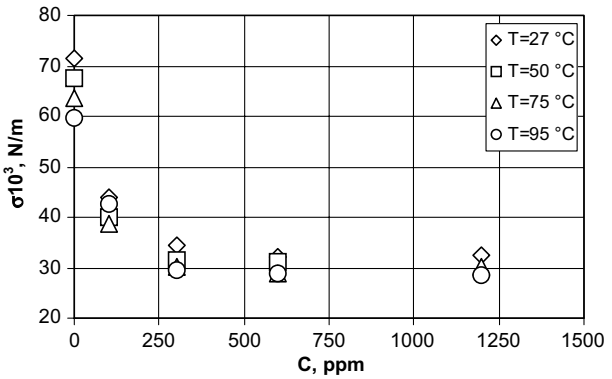

Fig. 2. Surface tension of surfactant solution versus a concentration at different temperatures.

a gear pump, 2. The flow rate was regulated by valves and a bypass line, 3, and measured by an orifice, 4. After leaving the flow meter, water flows into the pipe at the bottom end, then reaches a two-phase mixer, 5. Air is supplied from pressure tank, 9. The air flow rate was regulated by valve, 8, and measured by reometer, 7, at low gas rate and anemometer, 6, at middle and high flow rates. The air is introduced in the mixing chamber continuously through a porous layer. The mean pore diameter is 120 μm. Two phase mixture flows upward into the test section, 11. This section is depicted in more detail in the Fig. 3b. At first, the air–liquid mixture passes over a transparent glass section, 1, serving for identifying the flow patterns by the high-speed video camera, 2. The pressure measurements were done by two high-accuracy pressure transducers, 3 and 4 at a

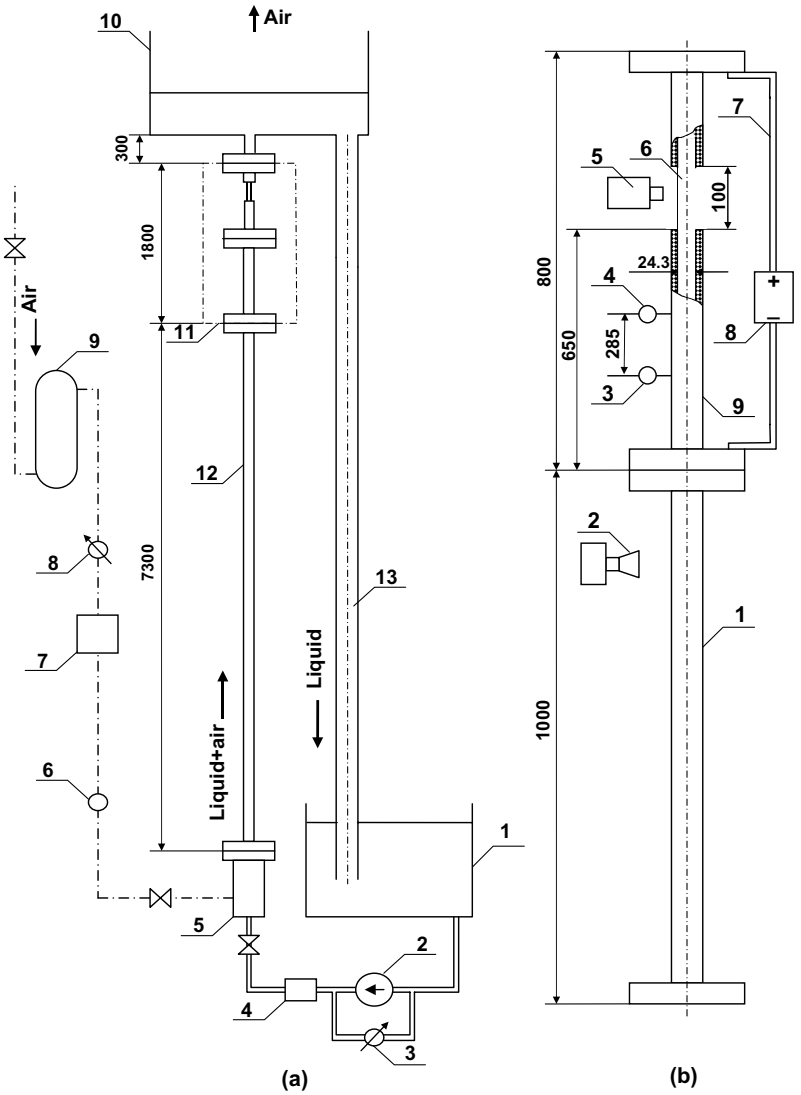

Fig. 3. Experimental set-up: (a) a schematic of the loop and (b) test section and measurement scheme.

distance 0.28 m apart. After passing through the observation section, the air–water mixture flows into the heated section, 9. This part of the test section is designed for temperature measurements. A constantan foil, 6, of 50 μm thickness is installed inside the polyethylene tube, which has window cut in its wall, to make the foil visible to the IR radiometer, 5. The window for IR observation is 100 mm long and 20 mm wide. The foil is coated, on the air side, by black mat paint of about 20 μm thickness. Constancy of heat flux is achieved by supplying DC current at up to 100 A from a power supply, 8 through cables, 7.

Then, the mixture flows upward to the upper tank. The air is released into the atmosphere, while the liquid returns to the entrance tank, on the lowest level. The main purpose of this configuration is to provide better separation of the air from the liquid, in order to obtain well-controlled flow rates of both phases. The experimental setup and measurement technique in more detail is described in Hetsroni and Rozenblit (2000).

2.3. Measurement techniques

A thermal imaging radiometer is used for the investigation of the temperature distribution on the heated foil of the test section. The temperature range of the radiometer is from −20 to 1500 °C, with a minimum

detectable temperature difference of 0.1 at 30 °C. Through calibration, the thermal imaging radiometer is very accurate in a narrow temperature range, giving the typical noise equivalent temperature difference (NETD) only, which is less than 0.2 °C (with the image average less than 0.05 °C). A typical horizontal resolution is 1.8 mrad or 256 pixels/line. The calibration of the radiometer was checked with a precision mercury thermometer placed in the water. Since the experiments were performed in two-phase flow, the heat transfer coefficient fluctuated in time. However, as was shown by Hetsroni and Rozenblit (1994), the temperature distortions and phase shift in temperature fluctuations on the heated foil begin at $f = 15$ Hz. In the present study the highest frequency of fluctuations did not exceed 6 Hz.

The hydrodynamic pattern in the pipes was studied by analyzing high-speed video images. The method is based on the detection of the edges of flow disturbance in a sequence of video frames. The motion of the flow disturbance was recorded by a high-speed motion analyzer, with recording rate up to 10 000 frames per second. The illumination was provided by a set of 500 W halogen lamps, mounted on a frame. Pictures were taken against a black background. In each run a sequence of at least 120 s was recorded. In the playback mode, typical flow patterns were frozen on the TV monitor and analyzed frame by frame.

The water flow was controlled by a valve and measured by a standard orifice plate with an accuracy of $\pm 1\%$. The air flow was measured by a reometer at low air rate and by a mass flowmeter with an accuracy of $\pm 1\%$ at middle and high flow rates. The pressure was measured by the pressure transducers with an accuracy of $\pm 1\%$ and response time of less than 5 ms. Electrical power was determined by means of a digital wattmeter with an accuracy of $\pm 0.5\%$. All data from sensors were transmitted to a PC, to be stored and analyzed.

2.4. Experimental procedure

An experimental run consisted of establishing the flow rate with and without air at different values of heat flux. Two-phase tests were conducted at constant liquid flow rates, with various air flow rates. The experiments were repeated to confirm their reproducibility. The heat transfer and flow parameters for each run were measured under steady-state conditions.

Video images were used for identifying the air–water flow regime. The transparent tube was illuminated by a halogen lamp. Pictures were taken against a black background.

For each run the pressure measurement was carried out for both the upper and lower pressure transducers. The pressure fluctuations were measured by sensors with response time less than 5 ms at sampling frequency of 500 Hz.

The measurement of average temperature of the heated wall and the heat transfer coefficient was done in the following way. We placed the scanner of IR radiometer at a distance of about 0.55 m from the side of the test section and measured the average temperature of the heater. These measurements were carried out both with air flow and without it. During each run, a sequence lasting at least 120 s was stored. Preliminary calculations (Hetsroni and Rozenblit, 1994) have shown that the difference between the temperatures of the two sides of the thin constantan foil was less than 0.1 °C. The estimated total heat losses were in the range of 12%, depending on the values of the heat flux.

The time-averaged heat transfer coefficient is defined as

$$h = q/(\overline{T}_w - T_f), \tag{1}$$

where q is the heat flux, $\overline{T}_w$ is the time-averaged wall temperature, T_f is the temperature of the water or air–water mixture, measured at $q = 0$.

3. Results and discussion

3.1. Flow patterns

An additive of surfactant to the carrying liquid causes drastic changes (Fig. 4) in the distribution of the gas phase inside the liquid. Flow regimes in both cases of the clear air–water mixture and the surfactant solutions may be classified as four patterns:

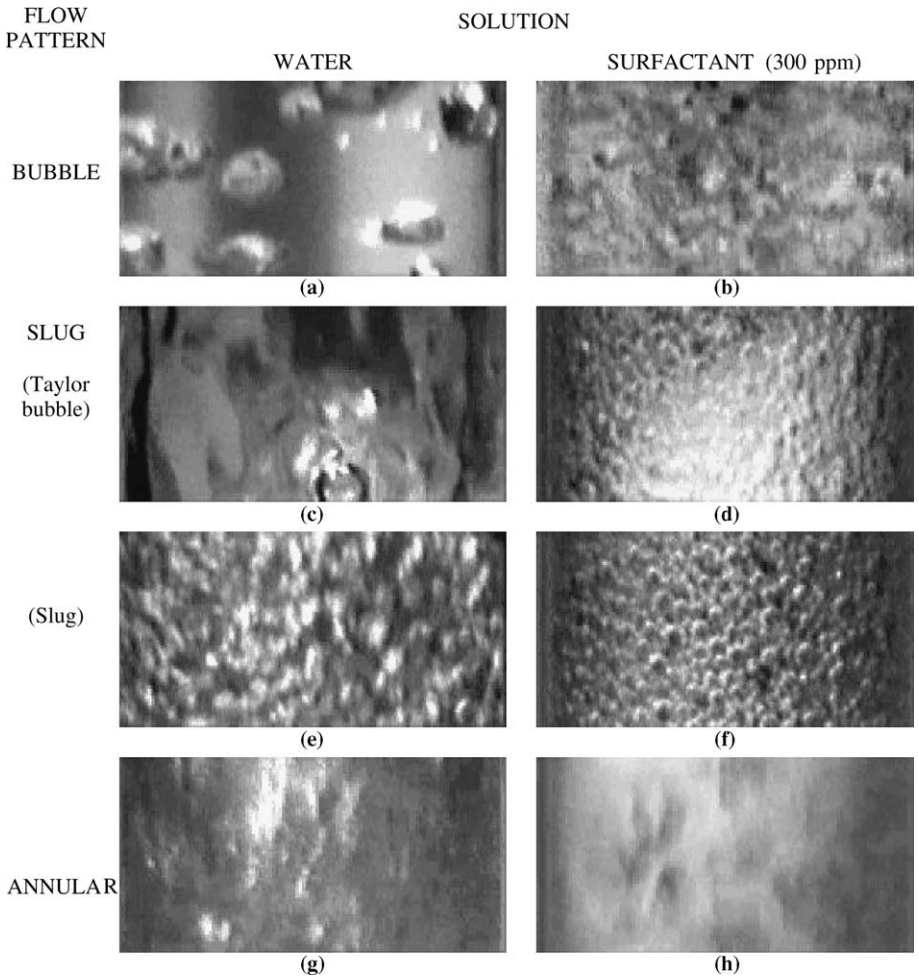

Fig. 4. The typical video images of flow structure at various flow regimes: bubble flow $U_{SG}/U_{SL} \approx 0.18$; slug flow $U_{SG}/U_{SL} \approx 1.0$; annular flow $U_{SG}/U_{SL} \approx 64$.

1. *Bubble flow* where discrete gas bubbles are dispersed in the liquid continuum. In small diameter tubes this regime exists at a high enough superficial velocity of the liquid that causes the mixture to have some frothy appearance. It is most pronounced at an addition of surfactant to the mixture. In clear air–water mixture the bubbles have an irregular shape (Fig. 4(a)). Fig. 4(b) depicts flow pattern of the 300 ppm surfactant solution under the same conditions. The surfactant additive reduces significantly the tendency of coalescence between air bubbles. The bubbles are smaller in size but much larger in number than in pure air–water mixture. In the surfactant solution, the shape of gas bubbles is closer to spherical, than for pure water. A decrease in the bubble size in two-phase pipe flow in the surfactant solution may be attributed to a decrease in the surface tension compared to that of clean water.
2. *Slug flow* where an increase in the gas rate causes some coalescence of bubbles resulting in the formation of bullet shaped Taylor bubbles (Fig. 4(c)), separated by slugs-liquid usually containing small gas bubbles (Fig. 4(e)). While the net flow is upward, the liquid between the Taylor bubbles and the pipe wall flows downward in the form of a thin falling film. In the solution of surfactant this film contains a large number of gas bubbles (Fig. 4(d)), because they characteristic size approaches the liquid film thickness. The air bubbles in the immediate region of a slug in surfactant solution (Fig. 4(f)) are also smaller in size and larger in number than in the clear air–water slug. The bubbles appear well packed in the slug liquid in a quite orderly manner.

3. *Churn flow* is seen as an important regime occurring between slug and annular flows, where the Taylor bubbles broke through the enclosing liquid to form a gas passage in the pipe centre. The video images in this regime are not having distinctive peculiarities and also represent gradual change from the images typical for the slug regime to annular regime.
4. *Annular flow* where the liquid continuum is mainly on to the pipe wall with a clear gas core in the pipe centre. There is no oscillatory up and down movement. However intermittently, liquid bridges are formed across the gas core. Frequently, the liquid surface has the wavy character. The gas core may contain the liquid droplets. We can see that typical image (Fig. 4(h)) of the film in surfactant solution becomes much foamier, than in clear air–water flow (Fig. 4(g)), because it includes enormous quantity of microscopic bubbles.

In the flow pattern definition we mainly followed classification described in Spedding et al. (1998a), where the authors carefully generalized the data on vertical two-phase flow. However we would have to combine semi-annular flow regime with annular flow, because the experimental definition of transitions between the semi-annular and churn flow and semi-annular and annular flow is very difficult in the surfactant solution, because of foaming.

3.2. Flow regime maps

There is no consensus yet on the most appropriate flow mapping parameters accounting for the phase properties and the tube diameter. In spite of this, it is interesting to compare the flow regime map for clear air–water flow with both the conventional map that has been adopted for vertical upward flow to verify setup and the map obtained for the same condition, but with the additive of surfactant to the air–water mixture.

Definition of the transition lines from one flow pattern to another was provided by analyzing of the pressure signals according to the method suggested by Tutu (1984) and used by us earlier (Hetsroni and Rozenblit, 2000). The analysis of high speed video sequences (up to 3000 frames per second) has served as supplementary tool in the situation where the boundary location was unclear.

Fig. 5(a) shows the regime map for clear air–water mixture obtained on this setup. Three transition lines (Taitel et al., 1980) for vertical upward two-phase flow are plotted on this map also. The first of them is the transition line from bubbly to the slug flow regime:

$$U_{SL} = 3.0U_{SG} - 1.15\left[\frac{g(\rho_L - \rho_G)}{\rho_L^2}\sigma\right]^{1/4}. \tag{2}$$

The second line is the transition from the slug to churn flow:

$$\frac{l_\varepsilon}{d} = 40.6\left(\frac{U_{SG} + U_{SL}}{\sqrt{gd}} + 0.22\right). \tag{3}$$

The third one is the transition from the churn to the annular flow:

$$\frac{U_{SG}\rho_G^{1/2}}{[\sigma g(\rho_L - \rho_G)]^{1/4}} = 3.1. \tag{4}$$

In Eqs. (2)–(4) U_{SG} and U_{SL} are superficial velocities of gas and liquid, respectively; ρ_G and ρ_L are average density of gas and liquid respectively, σ is the surface tension, l_ε is the entrance length, d is the pipe diameter and g is acceleration due to gravity. We can see that experimental data on air–water mixture are in good agreement with the theoretical prediction according to the Eqs. (2)–(4).

Fig. 5(b) presents the analogous map for the solution of surfactant with concentration of 300 ppm. We can conclude that in spite of drastic visual changes in the characteristic sizes of bubbles in the all flow regimes, the transition lines (calculated at decreased value of the surface tension for surfactant solution) are mainly consistent with the experimental data. The exception is some expanding the experimental data that may be identified as churn flow to the slug and to the annular flow at low gas velocities.

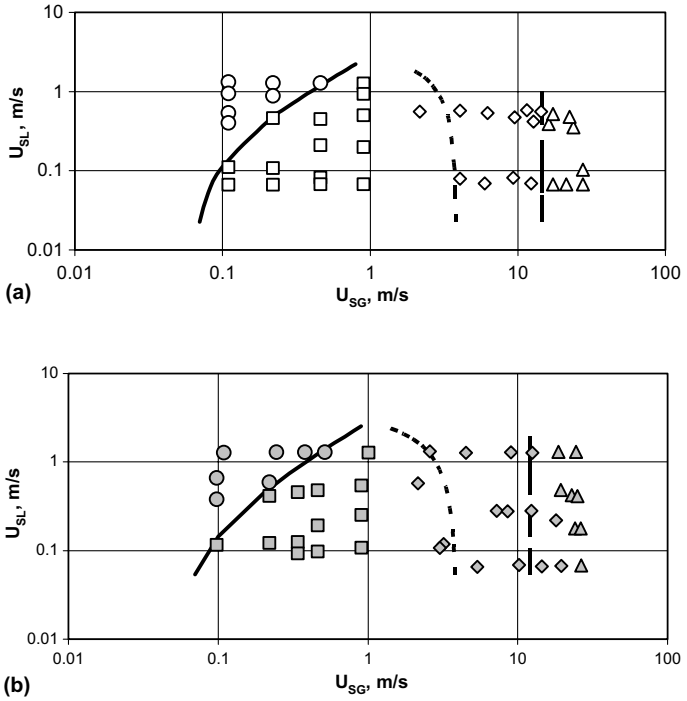

Fig. 5. The regime map. Symbols: (○) bubble flow, (□) slug flow, (◊) churn flow, (△) annular flow: (a) the clear air–water mixture (not filled symbols) and (b) the solution of the surfactant of 300 ppm with the air–water flow (grey symbols).

For the bubble/slug transition, such similarity could be predicted in advance since the rise velocity of the gas bubbles relative to the average liquid velocity is quite insensitive (Taitel et al., 1980) to changes of the bubble size.

Moreover, the deviation of transition lines for air–surfactant solution relative to air–water mixture, according to Eqs. (2) and (4) for bubble slug and churn annular regimes, is estimated as 20% whereas the surface tension of liquid is decreased twice. Similar results were obtained in the study of Sawai et al., 2004 on sodium oleate and CTAC surfactant solutions.

3.3. Pressure drop and drag reduction

The wall pressure fluctuations for vertical flow have been studied by Jones and Zuber (1975), Tutu (1984), Costigan and Whalley (1997), Spedding et al. (1998b) to define the boundaries of the flow regime transition. It was shown that careful definition of boundaries is an independent and difficult problem.

The measured pressure drops for upward gas–liquid flows are mainly an indication of liquid holdup and are weekly dependent on wall drag. It means that the total pressure drop does not reflect accurately the frictional component, particularly at low gas rates.

The typical pressure drop signals per the unit length for various flow regimes are shown in the Fig. 6 for both clear air–water flow and the surfactant solution of two concentrations of 100 and 300 ppm. It can be seen that the effect of surfactant on the pressure drop varies, depending on the flow regime. The surfactant increases an oscillatory component of the pressure drop signal for the bubble flow, whereas this component of the signal is essentially decreased for annular flow. The effect of surfactant on the pressure drop in the slug flow is only weakly distinctive. Fourier analysis (Fig. 7) of the pressure drop signal in this regime also shows insignificant changes in the pressure frequency and the intensity oscillations.

Fig. 8 gives experimental values of vertical total two-phase pressure drop per unit length depending on the ratio of superficial velocities for both clear air–water and surfactant at 300 ppm solution at two superficial velocities of liquid. We can see here that an addition of surfactant to two-phase flow decreases the total

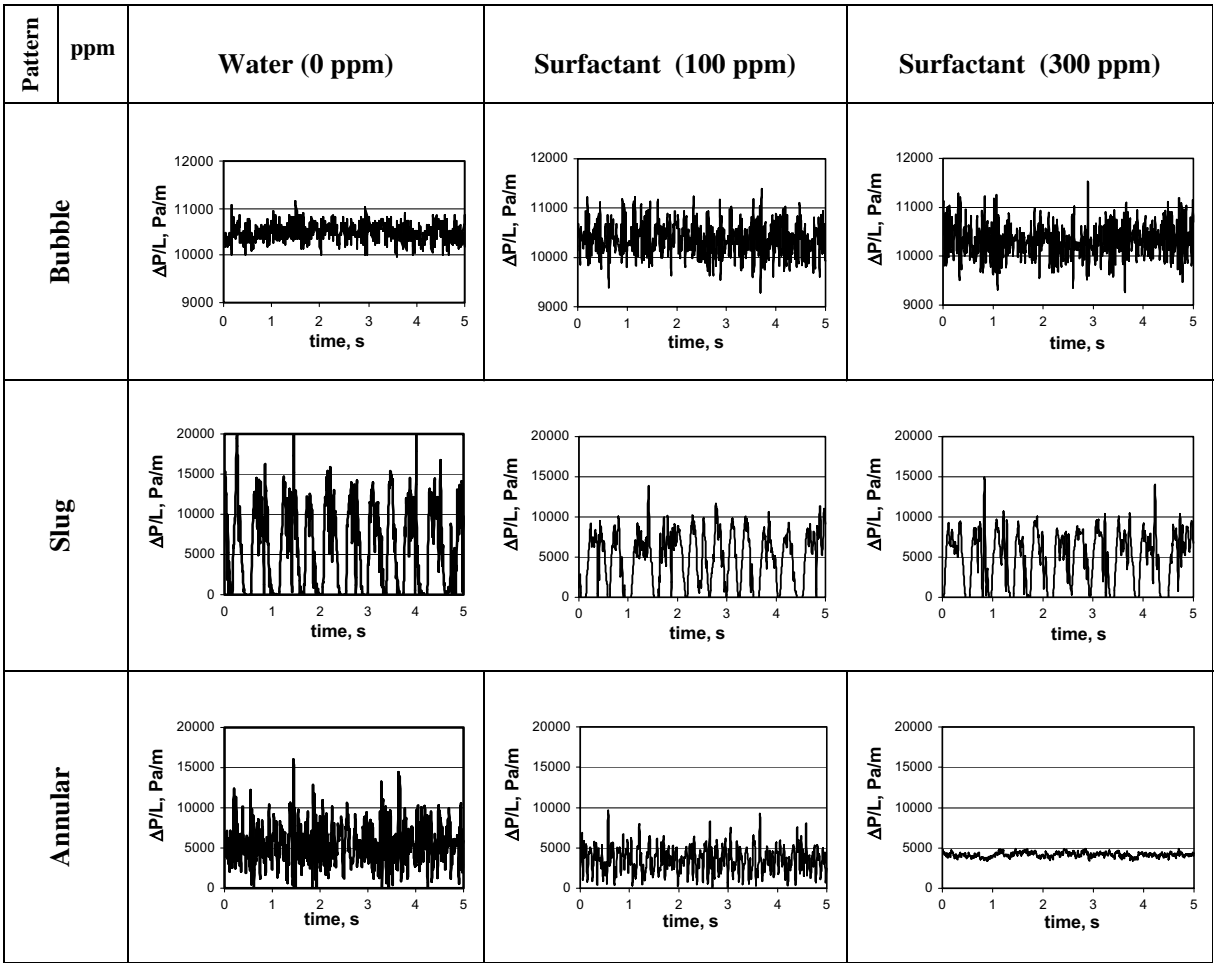

Fig. 6. The typical pressure drop signals: bubble flow $U_{SG}/U_{SL} \approx 0.18$; slug flow $U_{SG}/U_{SL} \approx 1.0$; annular flow $U_{SG}/U_{SL} \approx 64$.

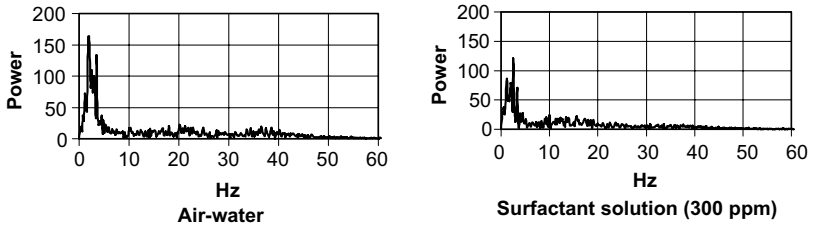

Fig. 7. Fourier analysis of pressure drop signal in slug flow.

pressure drop, as could be expected. This decrease is more pronounced at lower superficial liquid velocity. Quantitatively we will characterize the effect of the surfactant on the pressure gradient by the magnitude of pressure drop reduction (PDR) as

$$\mathrm{PDR} = \frac{(-\mathrm{d}P/\mathrm{d}x)_{\mathrm{w}} - (-\mathrm{d}P/\mathrm{d}x)_{\mathrm{s}}}{(-\mathrm{d}P/\mathrm{d}x)_{\mathrm{w}}}, \tag{5}$$

where $(-\mathrm{d}P/\mathrm{d}x)_{\mathrm{w}}$ and $(-\mathrm{d}P/\mathrm{d}x)_{\mathrm{s}}$ are the pressure gradients without and with surfactant addition. We can see (Fig. 9) that the PDR values increase with increasing superficial gas flow rates, arrive at their maximal values

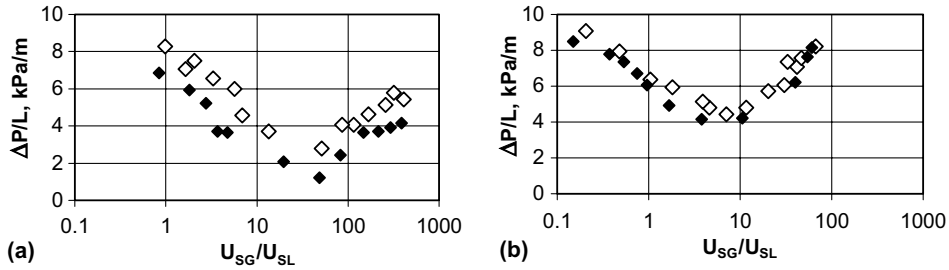

Fig. 8. The total two-phase pressure drop per the unit length depending on the ratio of superficial velocities at two superficial velocities of liquid. Symbols: (◊) clear air–water flow and (♦) the solution of surfactant of 300 ppm with air–water mixture.

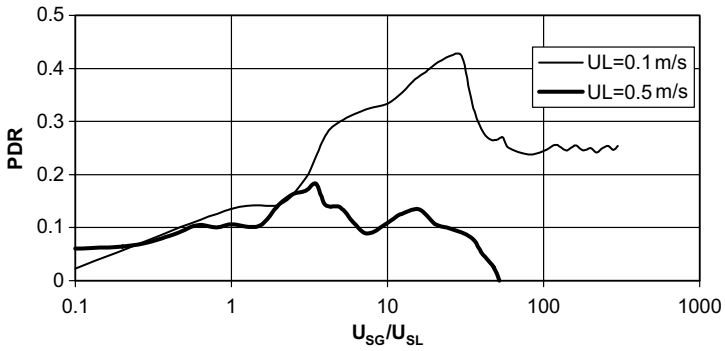

Fig. 9. The effect of superficial velocities ratio on value of PDR for two liquid velocities.

at slug-churn transition and decrease with further rise in gas flow rate. The maximal value of PDR is of 19% and 42% for the liquid superficial velocity of $U_{SL} = 0.5$ m/s and $U_{SL} = 0.1$ m/s respectively. These results agree well with the data on PDR of solution of air–water mixture with CTAC surfactant in the same diameter vertical tube obtained by Sawai et al. (2004). The authors divided the total pressure gradient into the frictional and gravitational pressure gradients. They found that decrease in the magnitude of the total PDR was caused mainly by the gravitational component, in another words by foaming in the liquid phase. Similar conclusions could be reached considering the data on PDR (Fig. 10) in the mixture of the clear water ($V_{SG} = 0$) and surfactant of 300 ppm concentration. We can see that the maximal value of PDR in this case is not over 0.5% at the liquid velocity $U_{SL} = 0.1$ m/s and 4% at $U_{SL} = 0.5$ m/s, whereas in the air–water flow with surfactant the magnitude of total PDR is considerably more.

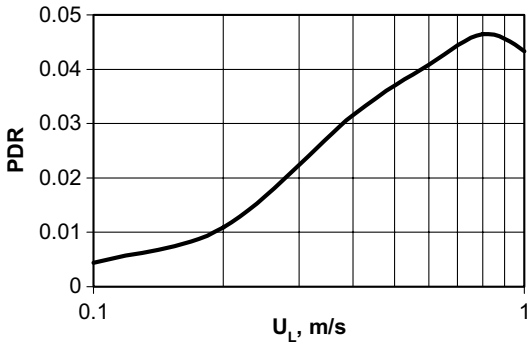

Fig. 10. The PDR dependence on the liquid flow rate in the mixture of the clear water ($U_G = 0$) and surfactant of 300 ppm concentration.

3.4. Heat transfer

The increase in the PDR value in a solution of clear water with surfactant is accompanied by a decrease in heat transfer. Fig. 11 shows the experimental dependence of the Nusselt number $Nu_L = \frac{h_L d}{\kappa_L}$ (where h_L is the heat transfer coefficient, d is the tube diameter and κ_L is the liquid conductivity) on the Reynolds number $Re_L = \frac{U_L d}{\nu}$ (where U_L is the average liquid velocity and ν_L is kinematic viscosity) for clear water and for surfactant solution of 100 ppm and 300 ppm. The dashed line in the graph is the Sieder–Tate equation for the heat transfer of liquid in the tube

$$Nu_L = 0.023 Re_L^{0.8} Pr_L^{0.4}. \tag{6}$$

We can see that an addition of surfactant to water causes a decrease in the value of the heat transfer coefficient. This fact is in good agreement with the data on the rise of PDR according to the data in Fig. 10.

The heat transfer in vertical air–water flows is defined not only by the friction value, but the by the gravitational component and distribution of gas phase in the liquid as well. Usually heat transfer in air–water flow is more intensive relative to the heat transfer in the clear water without gas phase. Several correlations have been used for two-phase heat transfer coefficients. Kudirka et al. (1965) and Dorresteijn (1970) correlated the heat transfer enhancement $\eta = h_{TP}/h_L$ over single-phase liquid heat transfer. Vijay et al. (1982) developed correlations based on the Lockhart–Martinelly parameter $\phi_L^2 = \Delta P/\Delta P_L$. The values of single phase liquid heat transfer coefficient h_L and pressure drop ΔP_L are determined from the standard heat transfer and friction factor correlations. The correlations in the form of a modification of the Sieder–Tate equation were proposed by Groothuis and Hendal (1959), Ravipudi and Godbold (1978), and Elamvaluthi and Srinivas (1983). In these works, the heat transfer experimental data and the data and correlations from various sources were compared. The excess form of the heat transfer coefficient in slug flow regime was introduced by Hetsroni and Rozenblit (2000).

Fig. 12 presents the relation of the two-phase Nusselt number versus the ratio of superficial velocities U_{SG}/U_{SL} for clear air–water flow and solution of the air–water mixture with surfactant of 300 ppm concentration at two different superficial velocities of liquid: 0.1 and 0.5 m/s. The experimental data for air–water mixture are in good agreement with the correlation (7) (dashed line in the graph 12) given by Kudirka et al. (1965)

$$Nu_{TP} = \frac{h_{TP} d}{k_L} = 125 \left(\frac{U_{SG}}{U_{SL}}\right)^{0.125} \left(\frac{\mu_G}{\mu_L}\right)^{0.6} Re_L^{0.25} Pr_L^{0.333} \left(\frac{\mu_B}{\mu_W}\right)^{0.14}, \tag{7}$$

where h_{TP} is heat transfer coefficient in two-phase flow, μ_G and μ_L are dynamic viscosities of gas and liquid respectively, μ_B and μ_W are dynamic viscosities of the liquid at the bulk and the wall temperatures, respectively.

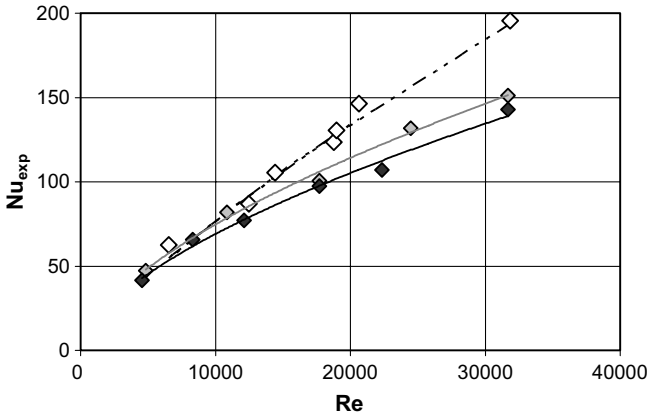

Fig. 11. The relation between the Nusselt number and Reynolds number in the mixture of the clear water ($U_G = 0$) and surfactant: water–hollow, surfactant of 100 ppm–grey; surfactant of 300 ppm–black symbols, respectively.

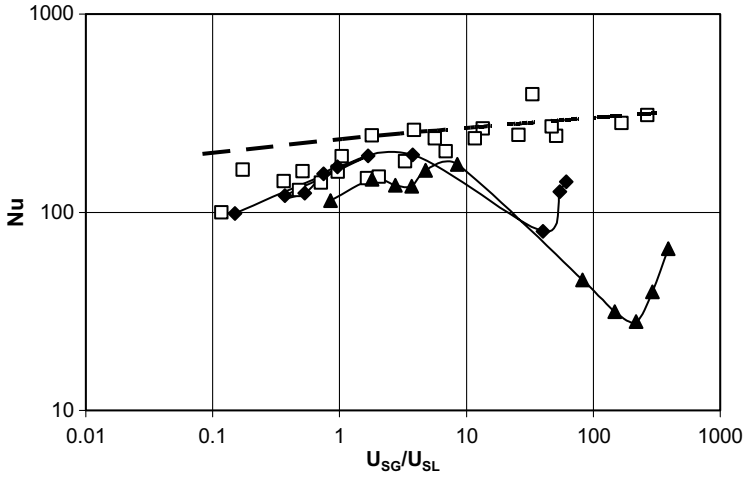

Fig. 12. The effect of the ratio of superficial velocities U_{SG}/U_{SL} on the two-phase Nusselt number for clear air–water flow and solution of the air–water mixture with surfactant of 300 ppm. Symbols: (□) air water mixture at two different liquid superficial velocities of 0.1 and 0.5 m/s; (▲) surfactant of 300 ppm at superficial liquid velocity of $U_{SL} = 0.1$ m/s; (♦) surfactant of 300 ppm at superficial liquid velocity of $U_{SL} = 0.5$ m/s; dashed line is the correlation of Kudirka et al. (1965).

An additive of surfactant to air–water mixture inconsiderable changes the heat transfer at low values of the ratio of superficial velocities $U_{SG}/U_{SL} \leqslant 1.0$ in the bubble and slug flow, whereas the surfactant drastically decreases the heat transfer in the churn flow regime, compared to the clear air–water flow. This phenomenon may be explained by two possible reasons. The first cause is some thickening of the film, because of huge number of small bubbles (Fig. 4(f, h)) emerged into the liquid next to the tube wall and cause some decrease in the average flow velocity. The second reason is a strong decrease in the value of thermal conductivity of the air–water mixture near the tube wall, because the gas has a much smaller thermal conductivity relative to the liquid one. The minimal value of Nusselt number for the solution of surfactant with air–water mixture occurs in the region of the transition from churn to annular flow. The rise in the gas flow rate is accompanied by further decrease in the gas bubbles diameter. The volume fraction of gas in the film progressively falls off, increasing both the heat conductivity of the film near the pipe wall and the liquid velocity. This phenomenon is accompanied by increasing the friction component of the pressure drop. Hence the heat transfer has again a tendency to rise in an annular flow regime. However it becomes lower than the one in clear air–water mixture.

4. Conclusions

Flow patterns, pressure drag reduction and heat transfer in vertical upward air–water flow with a surfactant, having negligible environmental impact, were studied experimentally in a tube of 2.5 cm in diameter.

Visual observations showed that the addition of surfactant reduced significantly the tendency of coalescence between air bubbles. The bubbles are smaller in size but higher in number than in pure air–water mixture at all flow regimes. The shape of bubbles is closer to spherical, than for pure water. The thin film around the Taylor bubble in the solution of surfactant contains a large number of gas bubbles at slug flow. The bubbles appear well packed in a quite orderly manner as in the slug liquid as well in the film in this flow regime. In the annular flow regime, the film in surfactant solution becomes much foamier, than in clear air–water flow.

The regime map for the solution of air–water mixture with surfactant of the 300 ppm concentration shows that in spite of drastic visual changes in the characteristic sizes of bubbles in the all flow regimes, the transition lines are mainly consistent with the experimental data obtained in clear air–water mixture. The exception is some deviation on the right of experimental data at small superficial gas velocity for the transition from the churn to annular flow.

The effect of the surfactant on the pressure drop varies depending on the flow regime. The surfactant increases an oscillatory component of the pressure drop signal for the bubble flow, whereas this component

of the signal is essentially decreased for annular flow. The effect of surfactant on the pressure drop in the slug flow is only weakly distinctive. An additive of the surfactant to two-phase flow decreases the total pressure drop, as could be expected. This decrease is more pronounced at lower superficial liquid velocity. The PDR values increase with increasing superficial gas flow rates, arrive at their maximal values at slug-churn transition and decrease with further rise in gas flow rate.

An additive of surfactant to air–water mixture inconsiderable changes heat transfer at low values of the ratio of superficial velocities $U_{SG}/U_{SL} \leqslant 1.0$ in the bubble and slug flow, whereas the surfactant drastically decreases the heat transfer in the churn flow regime relative to the clear air–water flow.

Acknowledgements

This research was supported by the Technion VPR fund. R. Rozenblit was supported by a joint grant from the Center for Absorption in Science of the Ministry of Immigrant Absorption and the Committee for Planning and Budgeting of the Council for Higher Education under the framework of the KAMEA Program.

References

Al-Sarkhi, A., Soleimani, A., 2004. Effect of drag reducing polymers on two-phase gas–liquid flows in a horizontal pipe. Chem. Eng. Res. Des. 82, 1583–1588.

Baik, S., Hanratty, T.J., 2003. Effects of a drag reducing polymer on stratified gas–liquid flow in a large diameter horizontal pipe. Int. J. Multiphase Flow 29, 1749–1757.

Costigan, G., Whalley, P.B., 1997. Slug flow regime identification from dynamic void fraction measurements in vertical air–water flows. Int. J. Multiphase Flow 23, 263–282.

Dorresteijn, W.R., 1970. Experimental study of heat transfer in upward and downward two-phase flow of air and oil through 70-mm tubes. In: Proceedings of 4th International Heat Transfer Conference, vol. 5, paper No. B5.9.

Elamvaluthi, G., Srinivas, N.S., 1983. Two-phase heat transfer in two component vertical flows. Int. J. Multiphase Flow 10, 237–242.

Groothuis, H., Hendal, W.P., 1959. Heat transfer in two-phase flow. Chem. Eng. Sci. 11, 212–220.

Hetsroni, G., Rozenblit, R., 1994. Heat transfer to a liquid–solid mixture in a flume. Int. J. Multiphase Flow 20, 671–689.

Hetsroni, G., Rozenblit, R., 2000. Thermal patterns on a heated wall in vertical air–water flow. Int. J. Multiphase Flow 26, 142–167.

Hetsroni, G., Gurevich, M., Mosyak, A., Rozenblit, R., Segal, Z., 2004. Boiling enhancement with environmentally acceptable surfactants. Int. J. Heat Fluid Flow 25, 841–848.

Jones, O.C., Zuber, N., 1975. The interrelation between void fraction fluctuations and flow patterns in two-phase flow. Int. J. Multiphase Flow 2, 273–306.

Kudirka, A.A., Grosh, R.J., McFadden, P.W., 1965. Heat transfer in two-phase flow of gas–liquid mixtures. Ind. Eng. Chem. Fundam. 4, 339–344.

Ohnuki, A., Akimoto, H., 1996. An experimental study on developing air–water two-phase flow along a large vertical pipe: effect of air injection method. Int. J. Multiphase Flow 22, 1143–1154.

Ravipudi, S.R., Godbold, T.M., 1978. The effect of mass transfer on heat transfer rates for two-phase flow in a vertical pipe. In: Proceedings of 6th International Heat Transfer Conference, Toronto, vol. 1, 505–510.

Sawai, T., Kaji, M., Urago, T., 2004. Effect of surfactant additives on pressure drop reduction in vertical upward two-phase flow. In: Proceedings of 5th International Conference on Multiphase Flow, Yokohama, Japan, May 30–June 4, paper No. 323.

Soleimani, A., Al-Sarkhi, A., Hanratty, T.J., 2002. Effect of drag-reducing polymers on pseudo-slugs-interfacial drag and transition to slug flow. Int. J. Multiphase Flow 28, 1911–1927.

Spedding, P.L., Woods, G.S., Raghunathan, R.S., Watterson, J.K., 1998a. Vertical two-phase flow. Part I: flow regimes. Trans. I. Chem. E 76 (Part A), 612–619.

Spedding, P.L., Woods, G.S., Raghunathan, R.S., Watterson, J.K., 1998b. Vertical two-phase flow. Part III: pressure drop. Trans. I. Chem. E 76 (Part A), 628–634.

Taitel, Y., Barnea, D., Dukler, A.E., 1980. Modeling flow pattern transitions for steady upward gas–liquid flow in vertical tubes. AIChE J. 26, 345–354.

Tutu, N.K., 1984. Pressure drop fluctuations and bubble-slug transition in a vertical two-phase air–water flow. Int. J. Multiphase Flow 10, 211–216.

Thwaites, G.R., Kulov, N.N., Nedderman, R.M., 1976. Liquid film properties in two-phase annular flow. Chem. Eng. Sci. 31, 481–486.

Vijay, M.M., Aggour, M.A., Sims, G.E., 1982. A correlation of mean heat-transfer coefficients for two-phase two-component flow in a vertical tube. In: Proceedings of 7th International Heat Transfer Conference, Munich, vol. 5, pp. 367–372.

Virk, P.S., 1975. Drag reduction fundamentals. AIChE J. 21, 625–656.

von Rybinski, W., Hill, K., 1998. Alkyl polyglycosides – Properties and applications of a new class of surfactants. Angew. Chem. Int. Ed. 37, 1328–1345.